Application of the Moving Boundary Truncation Method to Reactive Scattering: $H + H_2$, $O + H_2$, $O + HD$

Lucas R. Pettey* and Robert E. Wyatt

Institute for Theoretical Chemistry and Department of Chemistry and Biochemistry, The University of Texas, Austin, Texas 78712

Received: July 29, 2008; Revised Manuscript Received: September 28, 2008

The moving boundary truncation (MBT) method is a time-dependent adaptive method that can significantly reduce the number of grid points needed to perform accurate wave packet propagation while maintaining stability. This work presents a more robust variation of the method. Significant improvements have been made that allow the MBT method to be applied to any potential energy surface and used with any propagation method. The new variation of MBT is applied to the collinear $H + H_2$ reaction (using a LEPS potential) to demonstrate the stability and accuracy. Reaction probabilities are calculated for the three-dimensional nonrotating $O(^3P) + H_2$ and $O(^3P) + HD$ reactions to demonstrate that the MBT can be used with a variety of numerical propagation techniques.

1. Introduction

A very active area of research in chemical dynamics is the accurate and efficient calculation of quantum effects. There are many methods available to calculate quantum dynamics such as finite differencing,[1,2]fast Fourier transforms (FFTs),[3,4] basis set expansions,[5−10] the quantum trajectory method (QTM),[11−14] and trajectories with an approximate quantum force (AQF).[15−19] Methods based on finite differencing and basis set expansion were among the first applied to numerical integration of the time-dependent Schrödinger equation. The methods can be accurate, but they are usually inefficient due to conditions such as grid spacing or number of basis functions required for stability. Perhaps one of the most popular methods currently in use is the split operator method based on the FFTs.[3,4] FFT methods are accurate and can be quite efficient, but generally are limited to time-independent Hamiltonians and often require the use of unnecessary grid points. FFT based methods are also best when the kinetic energy transform from coordinate to momentum space is straightforward. In cases where the transform is not simple, such as the angular coordinate in cylindrical or spherical coordinates, FFT methods are coupled with basis set expansions. This can dramatically reduce the efficiency. Trajectory methods such as QTM[11−14] and AQF[15−19] can rival the efficiency of FFT based methods. The main reason trajectory methods can be so efficient is that only the points of interest are used in the calculation. In quantum trajectory methods, however, difficulties can arise in calculating certain quantum effects such as nodes and interferences in the wave function. Resolving exact quantum effects such as resonances and nodes using techniques like hybrid methods,[20,21] arbitrary Lagrangian−Eulerian (ALE) grids,[22−25] covering functions,[26,27] and approximate quantum forces[15−19] has been the subject of a great deal of research.

Recently, a new adaptive method[28,29] for integrating the time-dependent Schrödinger equation was introduced that combines the advantages of quantum trajectory methods while maintaining the accuracy of fixed grid methods. The moving boundary truncation (MBT) method utilizes quantum trajectories at the edge of a fixed grid to determine the boundaries within which a wave packet is propagated. As the wave packet moves or spreads, the trajectories move also, altering the boundaries in such a way that the dynamics are correctly represented. It is important to note that the trajectories do not directly influence the wave function; they simply determine which fixed grid points are most important to the dynamics at that particular time. Also, unlike other adaptive grid strategies, only the boundaries are changed. This greatly reduces the computational time. The approach is similar to methods independently developed by McCormack[30] and Hartke.[31] In these methods, localized basis sets are added or eliminated based on fixed density parameters[30,31] or time-dependent density parameters relative to the current maximum density.[30] In MBT, quantum trajectories determine what grid points are added to or eliminated from the calculation. Since density is not conserved along a trajectory path and trajectory paths do not cross, the quantum trajectories create an adaptive density criterion in the selection of grid points while always remaining at the boundary of the wave packet. The MBT has been proven to be as stable and accurate as traditional grid based methods while remaining as efficient as quantum trajectory methods.[28,29] The MBT method has been successfully applied to scattering problems in up to three dimensions, such as an Eckart barrier coupled to one or two harmonic oscillators.

This paper is intended to introduce a new variation of the MBT and extend the method to reactive scattering potential energy surfaces. The collinear $H + H_2$ reaction is the first reaction to which the new variation is applied. This reaction is a classic test of new methods for calculating quantum dynamics in chemical systems. In order to demonstrate only the new variation of the MBT, similar numerical methods are used as in previous studies.[28,29] The MBT method is then applied to the three-dimensional nonrotating $O(^3P) + H_2$ and $O(^3P) + HD$ reactions. These reactions are important to the combustion process[32] and have been the subject of a great deal of experimental[32−37] and theoretical research.[18,19,37−39] Calculating the dynamics of these systems will demonstrate how the method is extended to more complex potential energy surfaces and how any numerical method can be used in conjunction with the MBT method. The next section will formally introduce some of the trajectory principles and how they are applied in the MBT. Section 3 introduces the new variation of MBT used in this

10.1021/jp8067014 CCC: $40.75
Published on Web 12/05/2008

work. Section 4 shows the results of the MBT method and compares them to traditional fixed grid methods for accuracy and efficiency. The paper concludes by summarizing the work and generalizing the MBT for future applications.

2. Background

Quantum trajectory methods are generally based on the quantum hydrodynamic equations of motion (QHEM). These equations are formulated by substituting the polar form of the wave function, $\psi(\mathbf{r}, t) = R(\mathbf{r}, t) \exp(iS(\mathbf{r}, t)/\hbar)$, into the time-dependent Schrödinger equation, and the real and imaginary parts are separated. Often for trajectories, the equations are set up in the Lagrangian frame where the grid points move according to their Lagrangian velocity, $\dot{\mathbf{r}} = \nabla S(\mathbf{r}, t)/m$. In this frame the equations of motion become

$$\frac{\mathrm{d}R(\mathbf{r}, t)}{\mathrm{d}t} = -\frac{1}{m}R(\mathbf{r}, t)\nabla^2 S(\mathbf{r}, t) \quad (1)$$

$$\frac{\mathrm{d}S(\mathbf{r}, t)}{\mathrm{d}t} = \frac{1}{2m}(\nabla S(\mathbf{r}, t))^2 - V(\mathbf{r}, t) + \frac{\hbar^2}{2m}\frac{1}{R(\mathbf{r}, t)}\nabla^2 R(\mathbf{r}, t) \quad (2)$$

The first equation (eq 1) is the quantum continuity equation, so-called because it resembles the continuity equation from classical fluid dynamics. The second equation (eq 2) is the quantum Hamilton−Jacobi equation. This is exactly like the classical Hamilton−Jacobi equation except for the third term. This term is called the "quantum potential" since it is the only term that explicitly involves $\hbar$ and encompasses all quantum effects. It should be noted that the quantum potential varies with $1/R$. As a result, the quantum potential may become infinite at nodes in the wave function. Quantum trajectories ultimately never cross nodes, but as they approach a node, or near an area where the amplitude becomes small, the quantum hydrodynamic equations may become unstable.

The "node problem" is not an issue in MBT because the trajectories are only applied at the boundaries of the wave packet where the function is smooth. The real and imaginary parts of the wave function, A and B, are propagated using conventional grid methods. In order to apply MBT, an N-dimensional fixed grid is generated. For the purpose of this study, grid spacing is constant, but there is no evidence to suggest that an adaptive grid would be unstable. A minimum threshold for probability density is established, usually between 10^{-4} and 10^{-6}. Trajectories are placed at the points where the density is equal to the threshold. Since most numerical methods have some instability near the boundaries, a buffer of fixed grid points past the trajectories is included in the calculation. In the first example presented below, the buffer is 3 grid points, and it is 10 grid points in the second example. Appropriate boundary conditions are applied as if the grid terminated after the buffer points. The wave function is propagated one time step by any numerical method of choice. The trajectories are then propagated for one time step. The boundaries of the fixed grid are then adapted according to the new positions of the trajectories. New grid points are added or subtracted in order to maintain the appropriate buffer points based on the new positions for the trajectories. The process of continually adapting the boundaries of the fixed grid according to the motion of the trajectories is repeated until the desired number of time steps have been propagated.

In the original formulation of MBT,[28,29] the derivative propagation method (DPM) was used to move the trajectories at the boundaries and the wave function was propagated through finite differencing. A full explanation of DPM can be found in the literature such as the original paper by Trahan et al.[40] or Wyatt's book.[11] To summarize DPM, the spatial derivative operator is applied to both sides of eqs 1 and 2. The order of differentiation is then changed on the left-hand side of both equations. This generates a set of equations for propagating the first spatial derivative. The equations for propagating the first derivative are "upcoupled" to second and higher spatial derivatives. This "upcoupling" creates an infinite hierarchy of equations of motion. The hierarchy is terminated at a given order of derivative by assuming that the solution fits a polynomial expansion and derivatives of higher order than the polynomial are zero. The advantage of DPM is that each of the trajectories can be propagated independently while still carrying nonlocal information in the higher order derivatives that follow along with the trajectories.

Unfortunately, DPM is not applicable to all potential energy surfaces. For example, an attempt was made to propagate boundary trajectories on the collinear $H + H_2$ LEPS surface by Sato.[41] The trajectories are initially placed at the points where the density of a wave packet centered at [6.2, 1.4] has decayed to a value of 10^{-4}. In less than 1 fs of propagation time, the DPM trajectories begin to cross and do not follow the contours of the potential surface or the motion of the wave packet being propagated on the fixed grid. Exactly why these trajectories fail is the subject of current research. A new method for propagating the boundary trajectories has been developed in this work so that the MBT can be applied to an arbitrary potential energy surface.

3. Moving Boundary Truncation on Arbitrary Boundary Surfaces

In order to apply the MBT to arbitrary boundary surfaces, a propagation scheme similar to the QTM[11−14] is introduced for the trajectories. In QTM, a moving weighted least-squares (MWLS) fitting procedure is used to determine∇S and as such the Lagrangian velocity for the trajectories. In MBT, the trajectories may be too far apart to apply a MWLS fit using only the information carried by the trajectories. They are, however, always near underlying *fixed grid points* that carry the necessary information. Indeed, in MBT, the trajectories do not need to carry *any* information other than their position at each time step as all of the information needed to propagate both the wave packet and the trajectories is embedded on the fixed grid. The new method presented below exploits this advantage.

In order to calculate the velocity for a trajectory, the nearest fixed grid point is determined. Then all of the grid points within a predetermined distance are included in a least-squares fit of S in a similar fashion to QTM. The main difference is that the fixed grid points carry the wave function in the Cartesian form, $A + iB$, rather than the polar form, $R \exp(iS)$, as is the case in QTM. The S function is calculated by taking $\tan^{-1}(B/A)$ at the fixed grid points that will be used in the moving weighted least-squares (MWLS) fitting. This leads to the relative S, which may contain "saw tooth" features, due to the periodic nature of the $\tan^{-1}(B/A)$ function. Since only the gradient,∇S, is needed for the trajectory velocity, a constant can arbitrarily be added to pieces of S without affecting the derivative. Specifically, each time the S function "jumps", $\pi/2$ is added or subtracted so that continuity is preserved. Detecting the jumps is straightforward at the edges of the wave packet since S is generally smooth. The smooth S that is generated differs from the absolute S only by a constant; the slope of S is preserved, which is the only quantity of interest for calculating the gradient,∇S. The MWLS

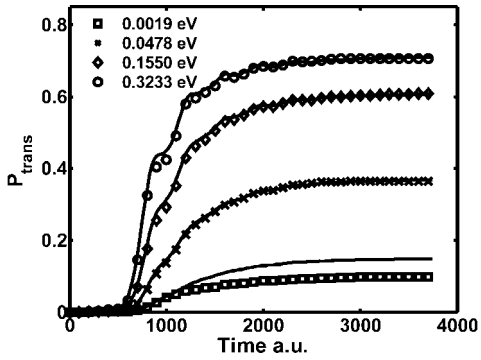

Figure 1. Transmission probabilities for the collinear H + H_2 reactions for various initial kinetic energies. The markers indicate the MBT calculation, while solid lines indicate the full fixed grid solutions. The difference in results can be reduced by moving the initial trajectory positions further from the center of the initial wave packet.

fitting procedure is applied to the new smooth S as outlined in the QTM. The∇S determined by MWLS is used to generate the Lagrangian velocity of the trajectories, and the trajectories can then be propagated in time.

One issue that can occur using this scheme is spreading or compression of the trajectories. When spreading occurs, the edges of the grid may not be correctly chosen. When compression occurs, more trajectories than are necessary to determine the edges of the fixed grid are being propagated. As a solution, the trajectories are periodically checked to ensure they are within a minimum and maximum distance of each other. Trajectories can be discarded and created as desired because all the information needed for propagation is being carried by the fixed grid.

4. Results and Discussion

A. Collinear H + H_2. The first application of the generalized MBT is the collinear H_A + H_BH_C reaction on the LEPS surface.[41] The wave function dynamics are solved in the Jacobi coordinate system where R is the distance between the incoming H_A atom and the center of mass of the reactant diatomic and r is the internuclear separation of the diatomic. The initial wave packet is the product of a Gaussian wave packet in R and the ground state of a Morse oscillator in r:

$$\psi(R, r, t=0) = \sqrt{\frac{\alpha}{\pi}} \exp\left[-\frac{\alpha}{2}(R-R_0)^2 - ip(R-R_0)\right] \phi_0(r) \quad (3)$$

The initial parameters for the wave packet in atomic units are $\alpha = 8.0$, $R_0 = 4.5$, and $p = [-4.875, -0.375]$, and ϕ_0 represents the ground state of the H_2 Morse oscillator centered at $r = 1.400\,83$ au. The wave function is propagated on a fixed grid with spacing $\Delta R = \Delta r = 0.05$ au, and the trajectories are started at points where the density of the initial wave packet has decayed to 10^{-4}. The numerical methods used to propagate the wave function are similar to those of previous work:[28,29] fourth-order finite differencing is used to calculate the kinetic energy operator, and a second-order leapfrog method is used to advance the wave function in time with a time step of $\Delta t = 0.25$ au. The transmission region for this example is all points $[R, r]$ where the distance from H_A to H_B is less than the distance from H_B to H_C. The transmission probability is calculated from the following integral: $P_{\text{trans}} = \int\int_{H_AH_B<H_BH_C} \psi^* \psi \, dR \, dr$.

Wave packets with various initial kinetic energies were propagated for 90.75 fs, and the results are summarized in Figure 1. The transmission probabilities of the MBT propagation are compared to those using a fixed grid whose boundaries are fixed at the minimum and maximum values achieved in each degree of freedom, $[R, r]$, by the MBT solution. The two methods are in excellent agreement. The MBT produces transmission probabilities that differ by only 1.13% for the highest three initial kinetic energies. The MBT results for the lowest kinetic energy (0.0019 eV) differ by 32%. If the trajectories are started at density values of 10^{-6} rather than 10^{-4}, the error is reduced to 10.21%, and if the initial trajectories are moved to density values of 10^{-8}, the error is reduced even further to 1.59%. Not only is the MBT extremely accurate in the converged transmission probability, but it captures the resonance patterns in transmission probabilities as seen in the 0.3233 and 0.1550 eV calculations.

While maintaining accuracy, the MBT is much more efficient than the full grid calculations. The full grid averaged 121 min and uses 1 074 316 grid points at each time step. The MBT calculations averaged only 15 min on the same computer, an 87.6% reduction in computational time. The reason for the MBT efficiency is shown in Figure 2. Although extra resources are necessary to propagate the trajectories, only 60 trajectories are needed initially as H_A approaches the diatomic (Figure 2a) moving toward $R = 0$ while the wave packet remains essentially a Gaussian in r. The 60 trajectories determine the boundaries of a fixed grid containing only 1514 grid points. A more detailed view of the initial wave packet is displayed in Figure 2b. This figure shows how the trajectories are initially started at equally spaced points corresponding to fixed grid points. Some of the trajectories are close together while others, particularly at the edges of r, are farther apart. Immediately after propagation begins, the algorithm will adaptively eliminate trajectories that are too close (<0.07 au) or add trajectories if the distance between existing trajectories is too large (>0.5 au). As the wave packet spreads into the product channel, more trajectories are added (Figure 2c), increasing the number to 234. The boundaries of the fixed grid are adapted according to the motion of the trajectories, increasing the grid size to 34 906 points halfway through the propagation. Once the transmission probability is converged (Figure 2d) and the propagation is complete, the wave packet has nearly bifurcated. The calculation finishes with 512 trajectories and 76 382 fixed grid points. The increase in the number of trajectories and grid points is nearly linear throughout the propagation of the wave packet. *The trajectories define the reactant and product channel with no advance information about the potential energy surface*. This means that no unnecessary grid points in the dissociative region are added into the calculations. Also, by calculating the wave function in the Jacobi frame, interference effects are resolved without numerical difficulties. If further propagation were desired, the trajectories could be used to create two separate wave packets as described in previous work.[28,29]

B. Three-Dimensional O + H_2 Reaction. The second example extends the MBT method to other numerical methods besides finite differencing. Specifically, a nonrotating atom + diatomic reactive system in three Jacobi coordinates $\{R, r, \theta\}$ is solved, where once again R is the distance between the incoming atom and the center of mass of the reactant diatomic, r is the reactant diatomic bond length, and θ is the angle between R and r. The total angular momentum is set to zero and the motion of the center of mass is eliminated so that the Hamiltonian becomes

$$\hat{H} = -\frac{1}{2M}\frac{\partial^2}{\partial R^2} - \frac{1}{2m}\frac{\partial^2}{\partial r^2} - \frac{1}{2\mu}\left(\frac{\partial^2}{\partial \theta^2} + \cot\theta\frac{\partial}{\partial \theta}\right) + \hat{V} \quad (4a)$$

or

$$\hat{H} = \hat{T}(R, r) + \hat{J}(\theta) + \hat{V}(R, r, \theta)$$

where the radial and angular kinetic energy operators are given by

$$\hat{T}(R,\ r) = -\frac{1}{2M}\frac{\partial^2}{\partial R^2} - \frac{1}{2m}\frac{\partial^2}{\partial r^2}$$

$$\hat{J}(\theta) = -\frac{1}{2\mu}\left(\frac{\partial^2}{\partial \theta^2} + \cot\theta\,\frac{\partial}{\partial \theta}\right) \tag{4b}$$

with the moment of inertia

$$\frac{1}{\mu} = \frac{1}{MR^2} + \frac{1}{mr^2} \tag{4c}$$

The specific reactive system is $O(^3P) + H_2(v = 0, j = 0) \rightarrow OH + H$ on the $^3A'$ potential energy surface originally developed by Rogers et al.[42] The potential surface was developed by first calculating the energy of 951 different geometries using a complete-active-space-self-consistent-field (CASSCF) internally contracted configuration interaction (ICCI) method. The energy for these geometries was then fitted to a surface using the generalized London−Eyring−Polanyi−Sato double polynomial (GLDP) method. This method creates a surface that is extremely accurate. The rms error is only 0.0117 eV with a maximum error of 0.0169 eV. The error is calculated by comparing CASSCF−CCI calculations to GLDP values for geometries not included in the original fitting. The surface that is generated, as shown in Figures 3a and 3b, contains three arrangement channels: one reactant $O + H_2$ channel and two product channels $OH + H$. The isotope effect is also examined by calculating the reaction $O(^3P) + HD(v = 0, j = 0)$. The product region of the potential surface is defined as the region where the OH (or OD) bond length is less than $3.5a_0$ and transmission probability is given by the integration $P_{trans} = \int\int\int \psi^*\ \psi \sin\theta\ d\theta\ dR\ dr$ over this region. There are two minimum energy paths (MEPs) corresponding to the collinear configurations ($\theta = 0$ and $\theta = \pi$) shown in Figures 3c and 3d. Moving along these MEPs, the maximum barrier height is 0.565 eV. The overall reaction is slightly endothermic, as the product channel of the MEPs is 0.11 eV higher in energy than the reactant channel. The dynamics on this potential energy surface have been studied using a variety of numerical methods including hyperspherical coordinates,[38] trajectory surface hopping,[39] and AQP.[18,19] In the work by Balakrishnan using hyperspherical coordinates,[38] the results were extended using a J shifting approximation to generate thermal rate constants in good agreement with experimental results. In the AQP studies,[18,19] classical trajectories were also examined to show the tunneling effects. The classical trajectories underestimated transmission probabilities for initial energies less than 1.4 eV, indicating that tunneling was significant.[18]

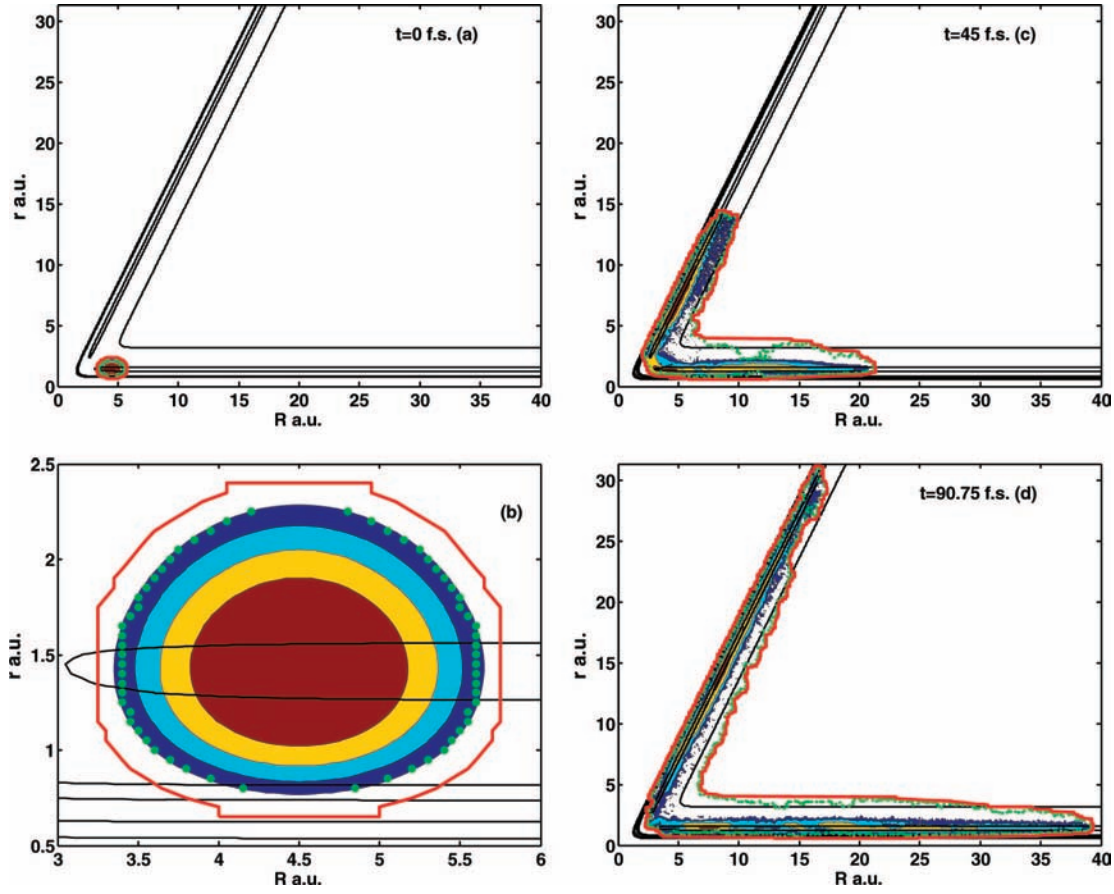

Figure 2. Wave packet propagation of the $H + H_2$ collinear reaction on the LEPS potential energy surface using the MBT method. The wave packet has an initial kinetic energy of 0.3233 eV. Filled contours represent the wave packet density ranging from 0.0001 in dark blue to 0.1 in red. Green points represent trajectory locations. Solid black contours represent the LEPS potential energy surface. Solid red lines indicate the boundary of the fixed grid used to propagate the wave packet. (a) Initial wave packet with 60 trajectories set at the edges of the 0.0001 contour. (b) Close-up of the initial wave packet and trajectories. (c) Wave packet after 45 fs of propagation. The trajectories have spread and their number has increased to 234 in order to correctly cover the fixed grid points needed to advance the calculation. (d) Final wave packet after transmission probability has converged. The number of trajectories has increased to 512.

The initial wave packet used for all calculations in this work is a product of Gaussians in {R, r}

$$\psi(R, r, t=0) = \sqrt{N}\exp[-\alpha(R-R_0)^2 - \beta(r-r_0)^2 - ip(R-R_0)] \quad (5)$$

with initial values of $\alpha = 4.0$, $\beta = 9.06$, $R_0 = 6.0$, $r_0 = 1.444$, and $p = [-18, -6]$ (all values are given in atomic units). In order to efficiently propagate the wave packet, the split operator method[3,4] is applied to the Hamiltonian as follows:

$$\psi_{t+\Delta t} = \exp\left(\frac{-i\Delta t}{2}\hat{J}\right)\times\exp\left(\frac{-i\Delta t}{2}\hat{V}\right)\times \exp(-i\Delta t\hat{T})\times\exp\left(\frac{-i\Delta t}{2}\hat{V}\right)\times\exp\left(\frac{-i\Delta t}{2}\hat{J}\right)\psi_t \quad (6)$$

A fast Fourier transform (FFT) is used to calculate the kinetic energy operator $\hat{T}(R, r)$, and the discrete variable representation (DVR)[5] is used for the rotational operator $\hat{J}(\theta)$. The grid for the FFT calculations is 256 × 256 with grid spacing $\Delta R = \Delta r = 0.08$. Sixty divisions of θ were used in the DVR calculations. Complete explanations of these two methods are widely available in literature, but summaries are provided here to emphasize how MBT can enhance their performance. The FFT transforms position space, [R, r], to momentum space, [P, p], thus simplifying the derivative operator to a multiplication. The transform is accomplished numerically by changing the integral to a discrete sum:

$$\psi_{j,k}(P,p) = \sum_{l=0}^{N_R-1}\sum_{m=0}^{N_r-1}\psi_{l,m}(R,r)\exp\left(\frac{-2\pi i}{N_R N_r}lm\right) \quad (7)$$

In eq 7, $\psi_{j,k}(P, p)$is the representation of the wave function in momentum space at point [P_j, p_k]. It is the weighted sum of the representation of the wave function in position space, $\psi_{l,m}(R, r)$, $l = 1,..., N_R$, $m = 1,..., N_r$, where N_R and N_r are the total number of points used in position space. At first glance, this would seem to be an ideal candidate for MBT, as the sum could be limited to only points within the boundary defined by the trajectories. As numerical algorithms for Fourier transforms have been developed over the years, however, symmetry properties of the transform have been exploited to reduce the overall number of terms that are actually calculated. For all of the available algorithms for FFT, the vector lengths in position space and momentum space must remain equal. This means that when MBT is applied to a FFT, either the number of points in momentum space is reduced to match the number of points in the truncated grid or the truncated grid can be padded with zeroes in order to maintain the appropriate number of momentum points required for a stable propagation. In the former case, the propagation quickly becomes unstable and inaccurate because the spacing in momentum is either too large or the minimum and maximum of the momentum space is limited. In the latter case, there is no efficiency gained by placing zeroes around the truncated grid. If a FFT algorithm was developed that could maintain the speed of symmetry based methods while

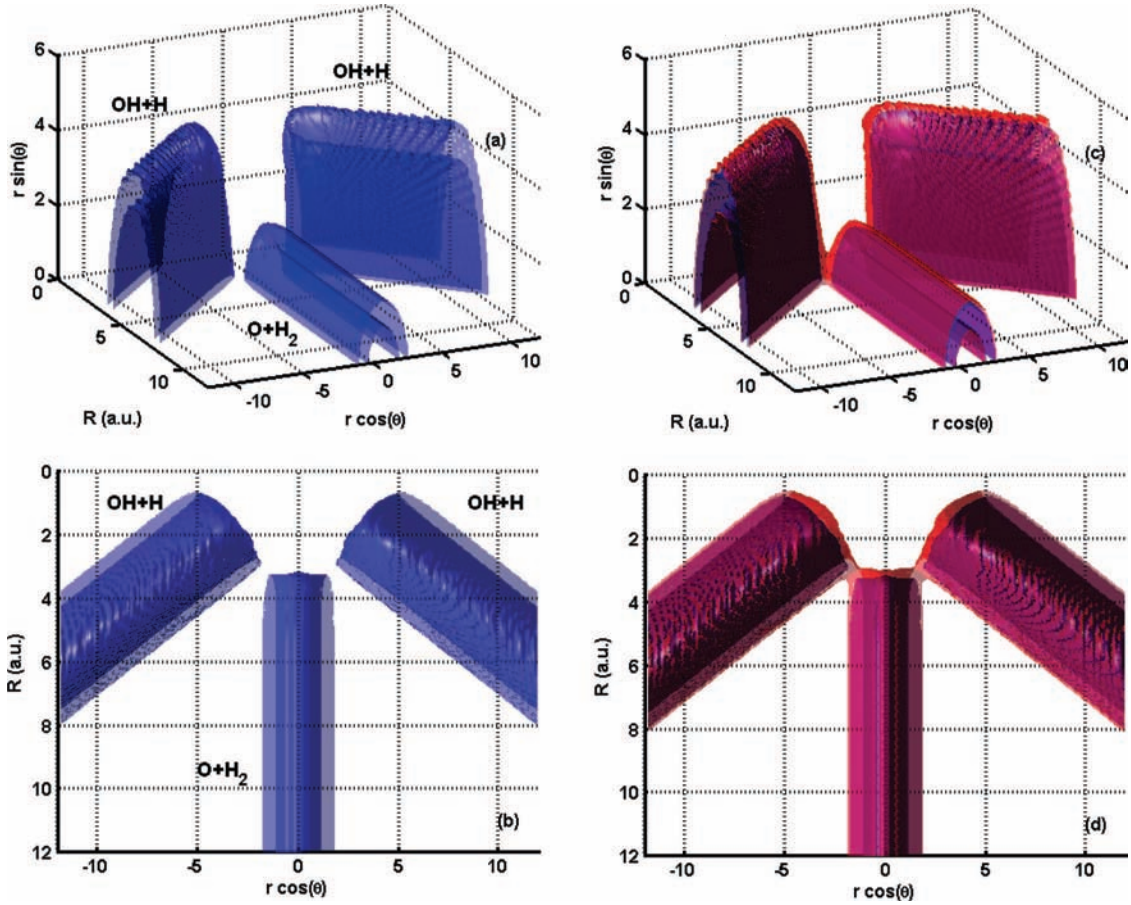

Figure 3. Isosurfaces of the $O(^3P) + H_2(v = 0, j = 0) \rightarrow OH + H\ ^3A'$ potential energy surface. (a) Reactant and product channels of the 0.5 eV potential surface. (b) Top view of (a), showing that the channels are not connected at this energy level. (c) Isosurfaces of the 0.5 eV (blue) and 0.75 eV (red) potential energy surfaces. At the angles near $\theta = 0$ and $\theta = \pi$, the reactant and product channels are connected through two barrier regions. (d) Top down view of (c).

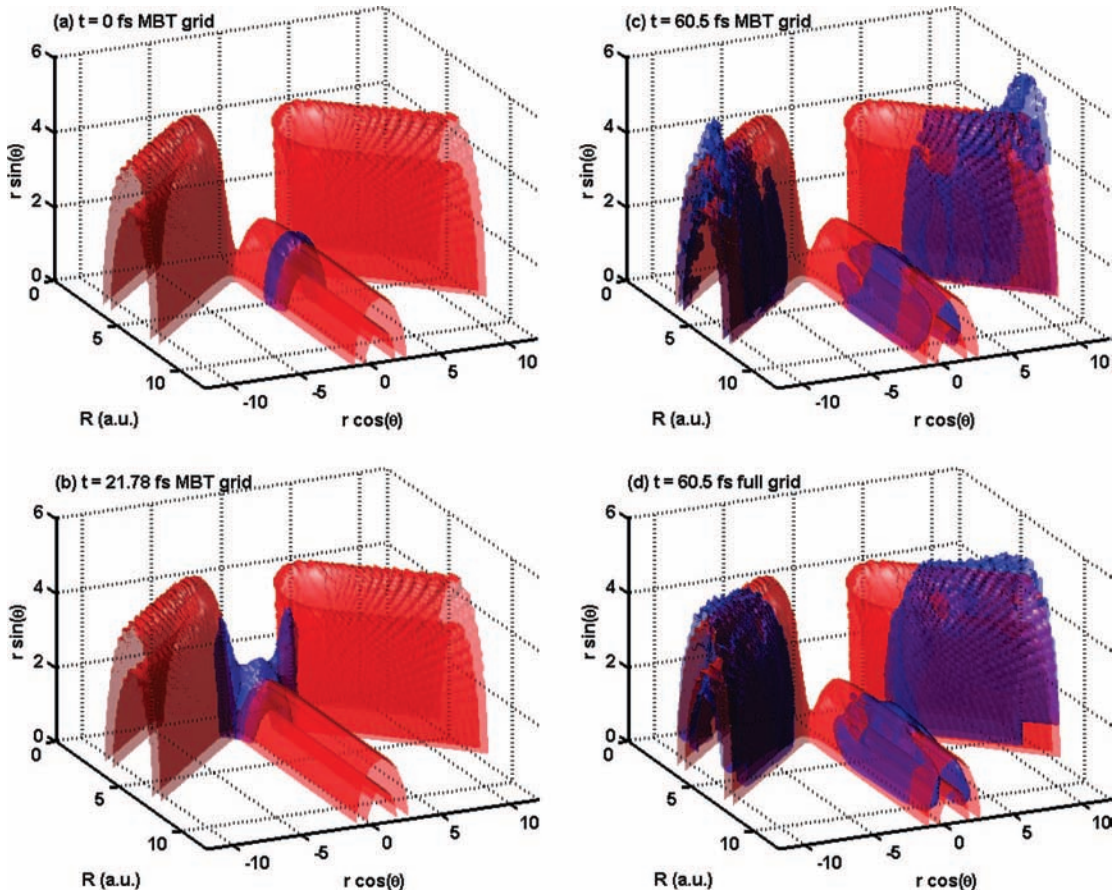

Figure 4. Wave packet propagation of the $O(^3P) + H_2(v = 0, j = 0) \rightarrow OH + H$ reaction on the $^3A'$ potential energy surface. The wave packet has an initial kinetic energy of 0.817 eV. Red isosurfaces indicate the potential energy surface at $V = 0.75$ eV. Isosurfaces of the wave packet at a density of 0.0001 are colored blue. (a) Initial wave packet. The points used in the rotational operator are only contained within the blue wave packet isosurface. The potential surface breaks into two tubes along $\theta = 0$ and $\theta = \pi$ at approximately $R = 2.5$ au.(b) Wave packet after 21.78 fs. The MBT has guided the wave packet correctly into the two product tubes. (c) Wave packet after transmission probability has converged (60.5 fs). The wave packet has fractured into three distinct parts, and MBT restricts the rotational operator to only these areas. The leading edge of the transmitted packets shows some numerical artifacts not present in the full grid. (d) Full grid wave packet after 60.5 fs.

allowing vectors of different lengths in position and momentum spaces, then MBT may be applicable to a FFT propagation.

The ideal application of MBT is for the rotational operator. The discrete variable representation (DVR) takes the wave function represented by a point basis and transforms it to a function basis.[5] The reason that the DVR is preferred over a FFT for the rotational operator is the cot $\theta\ \partial/\partial\theta$ term. Unlike the second derivative term in the kinetic energy operator, this term does not translate to a simple multiplication in momentum space. In DVR, a unique transformation matrix, Y, is used to transform the wave function from a number of points in θ to a basis set, usually that of a harmonic oscillator. In addition to being able to transform the wave function, any operator can also be transformed, $\hat{A}_{\mathrm{DVR}} = Y \hat{A}_{\mathrm{HO}} Y^{+}$. In this application of DVR, only points along θ are required and the transform is independent of $\{R, r\}$.

When MBT is applied to the mixed FFT−VR calculation, trajectories move along $\{R, r\}$ in discrete divisions of theta that will be used as DVR points. The minimum and maximum locations of the trajectories define a box in $\{R, r\}$. Only the points inside the box are used as DVR points in the transformation, and thus only these points have the rotational operator applied to them. Initially, there are 2760 trajectories divided evenly among the 60 θ divisions and placed in $\{R, r\}$ where the density of the wave packet has decayed to 10^{-4} (Figure 4a). This creates a box of 73 800 grid points in which the rotational operator is applied. As the trajectories move, the box of grid points moves with them, selectively applying the rotational operator only to the points where the density of the wave packet is significant. The number of trajectories and grid points used in the DVR stays relatively constant until the wave packet enters the transition state region at approximately 21 fs (Figure 4b). At this time, the trajectories have properly adapted the boundaries of the grid used in the DVR calculation so that the rotational operator is applied to produce the correct dynamics. After the wave packet has begun to enter the two product tubes, both the number of trajectories and the number of grid points in the DVR calculation increase linearly up to their final values, 6544 and 697 080, respectively, at the end of the propagation.

The advantages of MBT can be visualized in Figures 3 and 4. In these figures, the axes are cylindrical in that R lies along the x axis, r is the absolute distance from the x axis, and positive θ is counterclockwise rotation around the x axis. Examination of the potential isosurface for $V = 0.75$ eV, best seen in Figure 3c, shows that the rotational operator is not critical at early times as the potential energy is essentially independent of θ for the $O + H_2$ reactant channel. In the transition region at approximately $R = 3$ au, rotation is critical as the potential surface pinches and develops minima near $\theta = 0$ and $\theta = \pi$. The product channels then quickly form, and the potential surface expands to the entire range of θ. If rotation is neglected in the Hamiltonian, this important feature of the potential energy

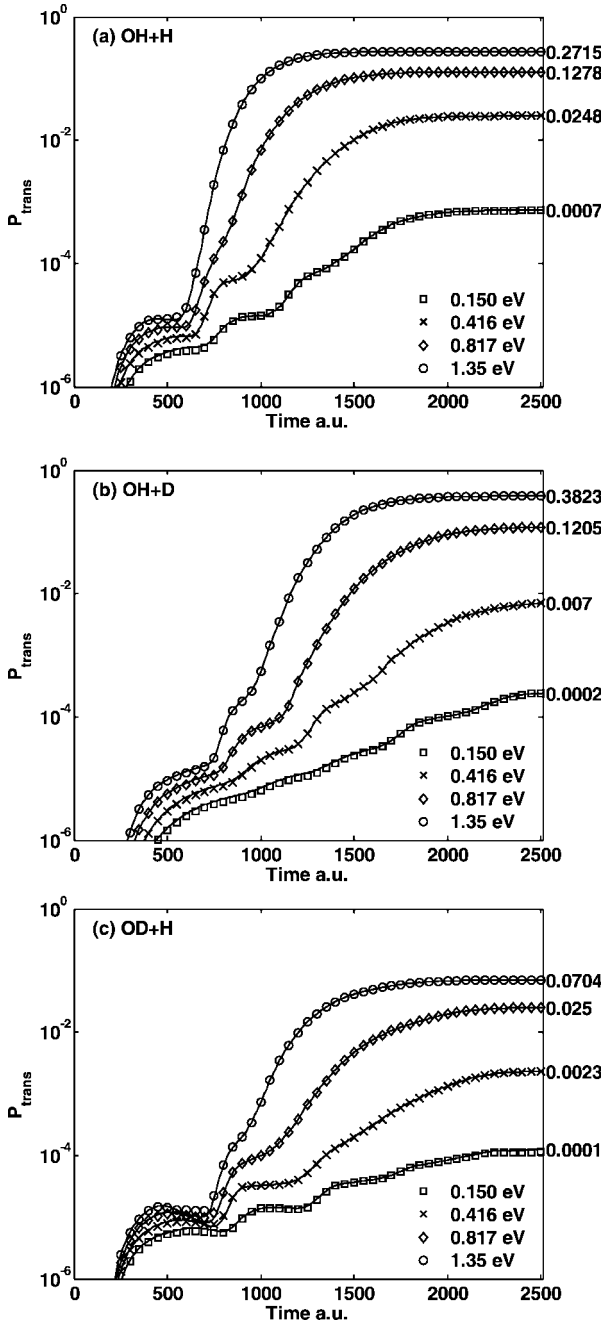

Figure 5. (a) Transmission probabilities for the $O(^3P) + H_2(v = 0, j = 0)$ reaction for various initial kinetic energies. The markers indicate the MBT calculation, while solid lines indicate the full grid solutions. Transmission probability (y axis) is on a logarithmic scale for clarity. Values on the right-hand side indicate the converged value of the full grid calculation. (b) The OH transmission probabilities of the $O(^3P) + HD(v = 0, j = 0)$. (c) The OD transmission probabilities of the $O(^3P) + HD(v = 0, j = 0)$.

surface is lost and calculated values for the transmission probability are significantly lower than the correct values. With MBT, the rotational effects are preserved but limited to the points inside the boundaries defined by the trajectories. As the packet enters the transition state region (Figure 4b), the effect of the rotational operator allows the packet to correctly spread through the $\theta = 0$ and $\theta = \pi$ regions. The trajectories continue to guide the MBT grid down the two product tubes until the transmission probability is fully converged, as shown in Figure 4c. Figure 4d shows the converged wave packet using the full grid. Comparing Figures 4c and 4d reveals that the wave packet on the MBT grid has a small number of artifacts on the leading edges of the transmitted portions that are not present in the full grid wave packet. This difference in the wave packets is only evident after the transmission probability has converged and does not appear to affect the stability or accuracy of the MBT calculation. The reason for the formation of these artifacts and their effect on detailed transmitted wave packet information will be explored in future research.

The performance of MBT is displayed in Figure 5. The transmission probability of both the MBT and the full fixed grid are nearly in exact agreement for the $O(^3P) + H_2(v = 0, j = 0)$ reaction (Figure 5a). The results are also in good agreement with those from other studies.[18,36] The error ranges from 0.15% to 2.03% with the largest error being at the lowest kinetic energy. Figures 5b and 5c show the two transmission probabilities for the $O(^3P) + HD(v = 0, j = 0)$ reaction. The dramatic influence of the rotational operator is demonstrated here by the large difference in transmission probability between the OH + D and OD + H products. The transmitted wave packet in the OH + D channel has twice the density of the OD + H wave packet in the 0.150 eV calculation. The difference in transmitted densities increases with initial kinetic energy as the 1.35 eV calculation results in an OH + D transmitted wave packet with more than five times the density of the OD + H transmitted wave packet. Once again the MBT is just as accurate as the full grid calculation with a maximum difference in OH + D transmission probability of 0.49% and OD + H transmission probability of 8.99% and capturing resonance patterns as transmission probability develops over time. The maximum errors are at the lowest energies. The OD + H transmission probability at the lowest initial energy is only 0.0128. The error at higher energies drops to 1% or less. The reason for the increased error at the lowest kinetic energy is that the trajectories have eliminated the low density edges ($<10^{-4}$) of the wave packet. These low density edges are responsible for tunneling effects. In a similar fashion to the collinear $H + H_2$, the initial trajectories could be extended outward to capture more of the initial wave packet and thus capture more of the tunneling. These excellent results are obtained much more efficiently than the full grid calculations. A full grid calculation takes an average of 212 min. The MBT only takes 75 min, a reduction of 65%.

5. Conclusion

In this work, a generalized method for applying the moving boundary truncation to arbitrary potential energy surfaces was presented. This time-dependent adaptive grid method relies on reconstructing a relative quantum action function S from the Cartesian wave function through $\tan^{-1}(B/A)$ and smoothing the periodic nature of the inverse tangent function. After smoothing, a moving weighted least-squares (MWLS) fit is applied to determine ∇S and move the trajectories along the boundary of the wave packet. This new variation was first successfully applied to the $H + H_2$ collinear reaction (using a LEPS potential surface) with finite differencing used to determine spatial derivatives. The MBT was then extended to more complex surfaces and numerical methods by calculating the $O(^3P) + H_2(v = 0, j = 0) \rightarrow OH + H$ reaction on the $^3A'$ potential energy surface. This example showed that MBT can be selectively applied to certain degrees of freedom in a multidimensional calculation using any grid based numerical method. This could prove useful in problems with a large number of degrees of freedom where certain degrees of freedom are calculated in total and others are truncated. The MBT method is not only efficient, but also calculates transmission probability very accurately. The

highest errors are always in low energy calculations. To increase accuracy for these situations, the initial trajectories can be set further from the center of the wave packet. Future research will focus on determining if there are subtle differences, such as phase information, between the full grid and MBT calculations as well as applying the MBT method to problems with more degrees of freedom and time-dependent potentials. FFT algorithms that can operate on unequal length vectors in position and momentum space will be explored to further exploit the efficiency of the method.

Acknowledgment. This research was supported in part by funding from the Robert Welch Foundation. The authors would also like to thank Sonya Garashchuk for supplying source code pertaining to the $O(^3P) + H_2(v = 0, j = 0) \rightarrow OH + H$ reaction.

References and Notes

(1) McCullough, A. E.; Wyatt, R. E. *J. Chem. Phys.* **1969**, *51*, 1253.
(2) McCullough, A. E.; Wyatt, R. E. *J. Chem. Phys.* **1971**, *54*, 3592.
(3) Leforestier, C.; Bisselling, R. H.; Cerjan, C.; Feit, M. D.; Friesner, R.; Guldberg, A.; Hammerich, A.; Jolicard, G.; Karrlein, W.; Meyer, H. D.; Lipkin, N.; Roncero, O.; Kosloff, R. *J. Comput. Phys.* **1991**, *94*, 59.
(4) Feit, M. D.; Fleck, J. A.; Steiger, A. *J. Comput. Phys.* **1982**, *47*, 412.
(5) Light, J. C.; Hamilton, I. P.; Lill, J. V. *J. Chem. Phys.* **1985**, *82*, 1400.
(6) Manthe, U.; Meyer, H. D.; Cederbaum, L. S. *J. Chem. Phys.* **1992**, *97*, 3199.
(7) Poirier, B.; Light, J. C. *J. Chem. Phys.* **1999**, *111*, 4869.
(8) Poirier, B.; Light, J. C. *J. Chem. Phys.* **2000**, *113*, 211.
(9) Yu, H. G. *J. Chem. Phys.* **2002**, *117*, 8190.
(10) Wang, X. G.; Carrington, T., Jr *J. Chem. Phys.* **2003**, *119*, 101.
(11) Wyatt, R. E. *Quantum Dynamics with Trajectories*; Springer: New York, 2005.
(12) Lopreore, C. L.; Wyatt, R. E. *Phys. Rev. Lett.* **1999**, *82*, 5191.
(13) Wyatt, R. E. *Chem. Phys. Lett.* **1999**, *313*, 189.
(14) Wyatt, R. E. *J. Chem. Phys.* **1999**, *111*, 4406.
(15) Garashchuk, S.; Rassolov, V. A. *Chem. Phys. Lett.* **2003**, *376*, 358.
(16) Garashchuk, S.; Rassolov, V. A. *J. Chem. Phys.* **2004**, *120*, 1181.
(17) Rassolov, V. A.; Garashchuk, S. *J. Chem. Phys.* **2004**, *120*, 6815.
(18) Rassolov, V. A.; Garashchuk, S.; Schatz, G. C. *J. Phys. Chem. A.* **2006**, *110*, 5530.
(19) Garashchuk, S.; Rassolov, V. A.; Schatz, G. C. *J. Chem. Phys.* **2006**, *124*, 244307.
(20) Hughes, K. H.; Wyatt, R. E. *Chem. Phys. Lett.* **2002**, *366*, 336.
(21) Babyuk, D.; Wyatt, R. E. *Chem. Phys. Lett.* **2004**, *387*, 227.
(22) Kendrick, B. K. *J. Chem. Phys.* **2003**, *119*, 5805.
(23) Pauler, D. K.; Kendrick, B. K. *J. Chem. Phys.* **2004**, *120*, 603.
(24) Kendrick, B. K. *J. Chem. Phys.* **2003**, *121*, 2471.
(25) Trahan, C. J.; Wyatt, R. E. *J. Chem. Phys.* **2003**, *118*, 4784.
(26) Babyuk, D.; Wyatt, R. E. *J. Chem. Phys.* **2004**, *121*, 9230.
(27) Babyuk, D.; Wyatt, R. E. *Chem. Phys. Lett.* **2004**, *400*, 145.
(28) Pettey, L.; Wyatt, R. E. *Chem. Phys. Lett.* **2006**, *4*−*6*, 424.
(29) Pettey, L.; Wyatt, R. E. *Int. J. Quantum Chem.* **2007**, *107*, 1566.
(30) McCormack, D. *J. Chem. Phys.* **2006**, *124*, 204101.
(31) Hartke, B. *Phys. Chem. Chem. Phys.* **2006**, *8*, 3627.
(32) Dixon-Lewis, G.; Williams, D. *J. Comput. Chem. Kinet.* **1977**, *17*, 1.
(33) Light, G. C. *J. Chem. Phys.* **1978**, *68*, 2831.
(34) Westburg, K.; Cohen, N. *J. Chem. Phys. Ref. Data* **1983**, *12*, 531.
(35) Presser, N.; Gordon, R. J. *J. Chem. Phys.* **1985**, *82*, 1291.
(36) Robie, D. C.; Arepalli, S.; Presser, N.; Kitsopoulos, T.; Gordon, R. J. *J. Chem. Phys.* **1990**, *92*, 7382–7393.
(37) Garton, D. J.; Minton, T. K.; Maiti, B.; Troya, D.; Schatz, G. C. *J. Chem. Phys.* **2003**, *118*, 1585–1588.
(38) Balakrishnan, N. *J. Chem. Phys.* **2003**, *119*, 195–199.
(39) Maiti, B.; Schatz, G. C. *J. Chem. Phys.* **2003**, *119*, 12360–12371.
(40) Trahan, C. J.; Hughes, K. H.; Wyatt, R. E. *J. Chem. Phys.* **2003**, *118*, 9911.
(41) Sato, S. *J. Chem. Phys.* **1954**, *23*, 592.
(42) Rogers, S.; Wang, D.; Kuppermann, A.; Walch, S. *J. Phys. Chem. A* **2000**, *104*, 2308.

JP8067014